Current Biology *16*, 345–358, February 21, 2006 DOI 10.1016/j.cub.2005.12.044

Article

A Quantitative Approach to the Study of Cell Shapes and Interactions during Early Chordate Embryogenesis

Olivier Tassy,[1,*] Fabrice Daian,[1] Clare Hudson,[2] Vincent Bertrand,[1,3] and Patrick Lemaire[1,*]

[1] IBDM (Institut de Biologie du Développement de Marseille)
UMR6216
CNRS-Université de la Méditerranée
Campus de Luminy
Case 907
13288 Marseille Cedex 9
France

[2] "Biologie du Développement" UMR 7009 CNRS
Universite Pierre et Marie Curie (Paris VI) Observatoire Océanologique
F-06230 Villefranche-sur-Mer
France

Summary

Background: The prospects of deciphering the genetic program underlying embryonic development were recently boosted by the generation of large sets of precisely organized quantitative molecular data. In contrast, although the precise arrangement, interactions, and shapes of cells are crucial for the fulfilment of this program, their description remains coarse and qualitative. To bridge this gap, we developed a generic software, 3D Virtual Embryo, to quantify the geometry and interactions of cells in interactive three-dimensional embryo models. We applied this approach to early ascidian embryos, chosen because of their simplicity and their phylogenetic proximity to vertebrates.

Results: We generated a collection of 19 interactive ascidian embryos between the 2- and 44-cell stages. We characterized the evolution with time, and in different cell lineages, of the volume of cells and of eight mathematical descriptors of their geometry, and we measured the surface of contact between neighboring blastomeres. These analyses first revealed that early embryonic blastomeres adopt a surprising variety of shapes, which appeared to be under strict and dynamic developmental control. Second, we found novel asymmetric cell divisions in the posterior vegetal lineages, which gave birth to sister cells with different fates. Third, during neural induction, differences in the area of contact between individual competent animal cells and inducing vegetal blastomeres appeared important to select the induced cells.

Conclusions: In addition to novel insight into both cell-autonomous and inductive processes controlling early ascidian development, we establish a generic conceptual framework for the quantitative analysis of embryo geometry that can be applied to other model organisms.

*Correspondence: tassy@ibdm.univ-mrs.fr (O.T.); lemaire@ibdm.univ-mrs.fr (P.L.)

[3] Present address: Department of Biochemistry and Molecular Biophysics, Columbia University, 630 West 168th Street, New York, New York 10032.

Introduction

The genomics revolution has produced a very large amount of molecular data, which are currently used in developmental biology studies to dissect the molecular pathways leading to the activation of specific developmental programs. Much of this effort is geared toward unravelling the molecular regulatory networks that preside over cell-fate specification [1, 2].

While fate specification is largely driven by transcriptional regulatory networks, it cannot succeed in the absence of a precise embryo topology. For example, in the case of inductions, it is crucial that the cells emitting a signal and those competent to respond to it be within signaling range. This may involve morphogenetic/migratory events and/or a careful segregation of competence factors and inducers in adjacent territories via oriented cell divisions. To fully understand an induction event, the identification of the inducers, competence factors, and downstream targets thus needs to be complemented by a detailed characterization of the geometry and spatial arrangement of individual tissues or cells in developing embryos. Except in few specific cases [3, 4], the mechanisms controlling cell geometry have, however, received little attention in metazoan embryos. There is a considerable gap between the extensive, quantitative molecular and expression data gathered in the genomics projects and the largely qualitative and coarse description of cellular or tissue geometry. Bridging this gap will involve the development of digital systems, or virtual embryos, to quantify cell morphology and spatial position and to integrate these data within molecular model organism databases.

Several ongoing projects use imaging technology to fulfil this aim. The principal project of interactive 3D embryos, the Edinburgh Mouse Atlas Project (EMAP [5]), allows the mapping of gene expression data in space. The various structures of the embryo are represented, and their spatial arrangement can be intuitively visualized. Quantitative measures of their geometry and spatial arrangement are, however, not provided. In contrast, the 3D-DIASemb project [6] was specifically developed to quantify cell motions and morphology in the simple embryos of the worm *C. elegans*. This system, however, is not interactive, does not provide a formal quantification of the interactions between cells, and is not connected to a model organism database.

To achieve a more integrated view of embryonic development, we developed a generic open source software named 3D Virtual Embryo. This software displays interactive three-dimensional embryo models with a level of resolution adaptable to the model organism of choice. It integrates a set of mathematical tools to quantitatively characterize the morphology, spatial

arrangement, and physical contacts between the anatomical parts composing the embryo. To relate geometry, anatomy, and molecular data, 3D Virtual Embryo was integrated as a module of an advanced model organism database, NISEED, we recently developed (O.T. et al., unpublished data).

To illustrate the potentialities of 3D Virtual Embryo, we first applied it to early ascidian embryos. Ascidians are model organisms of choice because their embryos develop with a small number of cells and an invariant lineage, allowing their study a cellular level of resolution. Furthermore, a large set of genomic data was gathered in recent years, including assembled sequences of two small and compact annotated *Ciona* genomes [7, 8], more than 700,000 ESTs, and expression patterns for around 20% of predicted protein-coding genes [9, 10]. Finally, the phylogenetic position of ascidians, which diverged from vertebrates near the root of the chordate tree, and the sharing of at least some of embryonic strategies with vertebrates [7] suggests that the study of these simple embryos will shed light on the more complex vertebrates.

Results

Construction of a Set of Virtual Cleavage-Stage Ascidian Embryos

We first designed a procedure to generate a collection of 3D models of embryos, made of individualized cells and covering pregastrula ascidian development. Because *Ciona intestinalis* embryos are small—140 μm—but only relatively transparent, we used two-photon confocal microscopy to image embryos, fixed between fertilization and the 44-cell stage, after fluorescent staining of blastomere cortices (Figure 1A). The resulting z-stacks of 2D optical sections (see Movie S1 and Figure S1 in the Supplemental Data available with this article online) were used to reconstruct embryo models. Several technologies can be used to represent biological objects, such as organelles, cells, or anatomical structures, in three dimensions. The EMAP Project chose a voxel (volumetric pixel) representation, which retains all the information from the image stack, but results in very large model files. 3D-DIASemb [6] made a different choice. Only the external envelope of biological objects is represented, by means of polygon meshes, a representation known as vectorial 3D. 3D Virtual Embryo uses this latter strategy to reconstruct the contour of each cell (Figures 1B–1E), which is subsequently named according to the ascidian nomenclature [11] (see Experimental Procedures). This leads to 3D files sufficiently small to be easily exchanged between labs or visualized on modest personal computers used by biologists. Additional subcellular components such as the cell nuclei can also be stained and included in the embryo model (not shown). For more complex embryos, in which a cellular resolution cannot be reached, higher-order structures such as tissues or organs can be individually reconstructed. With this procedure, we generated 19 interactive embryo models covering the egg, 2-, 4-, 8-, 16-, 24-, 32-, and 44-cell stages of *Ciona intestinalis* as well as a late 32-cell stage of *Halocynthia roretzi*. These embryos, as well as some reconstructed partial embryos, form the basis of the analysis below.

Visual Exploration of Virtual Embryos

Figure 2A presents the general interface of 3D Virtual Embryo. Interfaces in the right window provide textual information on selected 3D objects, such as cells or anatomical structures, and allow the user to place queries on them. The left window displays the 3D model uploaded by the user. When loaded into the software, each 3D object is given by default a translucent appearance, to provide a global view of the embryo and to simultaneously visualize fore- and background cells. The names of cells or anatomical structures defined at the time of embryo reconstruction are displayed as a list in the right-hand "Anatomy" panel. They are also displayed as 3D text objects placed at the center of gravity of each cell.

The embryo models are fully interactive. Each cell or structure can be individually selected, either by clicking on its 3D representation with the computer mouse or by selecting it by its name in the list of structures appearing in the textual right-hand Anatomy interface. The color, transparency (0%–100%), and appearance (translucent, opaque, wireframe, or points) of selected and unselected objects can be edited by using the "display settings" panel (Figure 2C).

These basic features permit the visualization of the shape of individual blastomeres. Although the outside appearance of *Ciona* embryos can be likened to that of a raspberry, Figure 2A illustrates the diversity of the shapes of individual cells. For example, at the late 32-cell stage, the animal blastomere a6.8 has a tall columnar shape, the vegetal blastomere B6.2 is large and compact, the posterior vegetal B6.3 blastomere is small and flattened, and B6.1 or A6.2 have complex shapes, with concave and convex surfaces. The precise shape of a cell or structure can be observed by selecting it and choosing a wireframe (Figure 2D) or point (Figure 2E) representation for surrounding unselected cells. Cells or structures can also be virtually ablated by showing unselected cells as opaque and hiding the selected object(s). This function allows the observation of inner embryonic structures (Figures 2F and 2G). Alternatively, the inner architecture of an embryo can also be revealed by virtually slicing it along one or several of its three axes (Figure 2H) or by displaying thin embryo slices (Figure 2I).

In addition to providing the qualitative description of the shape and position of individual blastomeres presented in this section, 3D Virtual Embryo was designed to provide a quantitative description of the shape of individual structures and of their relative spatial arrangements. The following sections present these functions, which can be accessed via the "Biometry" interfaces.

Quantitative Analysis of Cellular Geometry Suggests a Sophisticated Developmental Control of Cell Shape

To quantitatively describe the geometry of individual blastomeres and its evolution, we defined mathematical descriptors for the size, elongation, roundness, flatness, convexity, squareness, surface over volume ratio, and entropy of each cell (see Experimental Procedures). These measures involved the comparison of the object to its convex hull or to its best-fitting rectangular parallelepiped (bounding box). As expected, the shape of the bounding boxes is in keeping with the intuitive

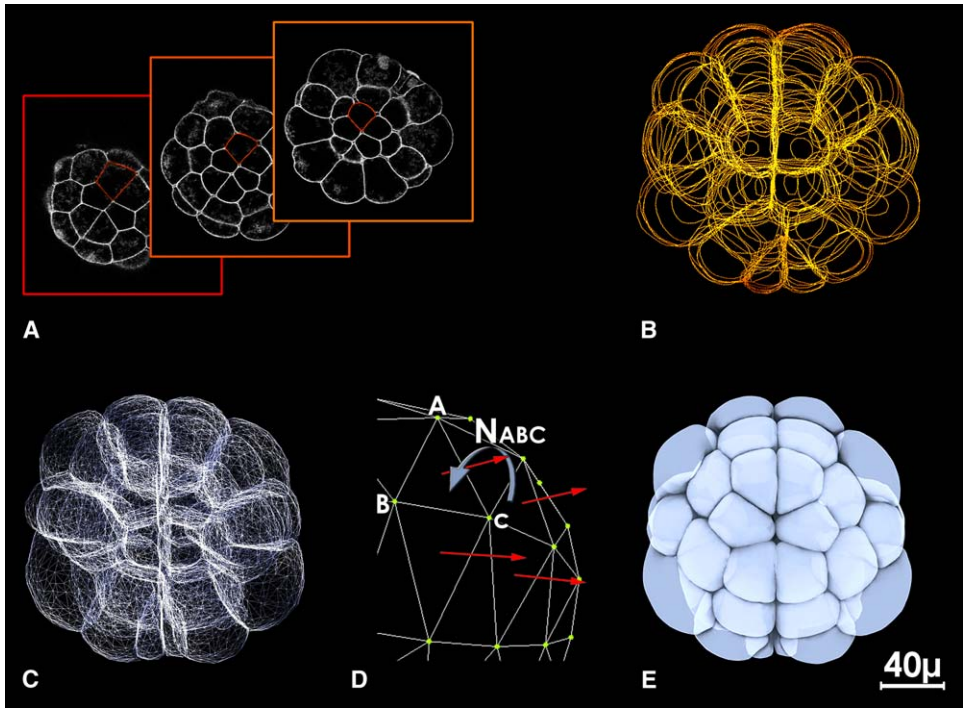

Figure 1. Reconstruction of 3D Embryo Models

(A) Examples of 2D confocal sections taken at different z values through a late 32-cell stage *Ciona* embryo fixed and stained with rhodamine-phalloidin.

(B) Animal view of the combined splines drawn around each cell contour on successive confocal images of a stack.

(C) Wire frame view of the reconstructed embryo.

(D) Schematic representation of the normal vectors associated to each triangle in the models. The direction of the normal for a triangle is determined by the order of the vertices.

(E) Embryo model displayed with a translucent texture.

description of the cells provided at the end of the first section for a mid-32-cell embryo (Figure 3A). a6.8 is bounded by a tall and narrow box, B6.2 by a square box, and B6.3 by a flat box. Computations of these geometry descriptors quantified the elongated character of a6.8, the compact character of B6.2, and the flattened shape of B6.3 at the mid 32-cell stage and more generally provided a geometrical "signature" for each blastomere (Figures 3B and 3C). Reconstruction of several sibling embryos at the early 32-cell stage revealed the consistency of this signature between embryos (Figure S2A–S2D). To test whether this signature was sufficient to unambiguously identify each cell in early embryos, we calculated for each embryo a distance matrix between cell shapes and represented the results as a tree (see Figure S3 for details of the computations and examples of the trees). In at least one reconstructed embryo of each of the 4-, 16-, 24-, and 32-cell stage, more than 75% of cells were found geometrically closest to their contralateral counterpart (Figure S3 and data not shown), suggesting that the descriptors provide adequate discrimination between cells at these stages. To assess the variability in cell shape between embryos, we analyzed four early 32-cell embryos, including three from the same batch of eggs. We found a variable number (6 to 14) of contralateral pairs of cells grouping together even between sibling embryos (see Figure S3). Thus, ascidian embryos, while generally bilaterally symmetrical, may tolerate some level of asymmetry. In the future, live imaging and reconstruction of additional embryos will allow this issue to be rigorously tested.

Comparing the descriptor values obtained at different stages for a given cell allows the user to plot their evolution and to compare it between cells or groups of cells. For instance, Figure 4A illustrates that the elongation of cells of animal and vegetal hemisphere is differentially regulated. Up to the early 32-cell stage, vegetal cells are on the whole slightly more elongated than animal cells. Animal cells then sharply elongate during the second half of the 32-cell stage, before contracting again at the 44-cell stage. Amusingly, between the early 32-cell stage and the mid 44-cell stage, the elongation factors of opposing animal and vegetal cells change in precisely opposite manner with time as exemplified for a6.8 and A6.1 on Figure 4B. This elongation is, however, not uniform among the cells of each hemisphere. Figure S4A illustrates, for instance, that between two representative early 32- and late 32-cell stage embryos, the a6.5 cell pair elongates significantly less than the other animal cells. Taken together, these findings suggest an elaborate developmental control of the shape of cells.

Regulation of Cell Volumes and Identification of Unequal Divisions

To test whether alterations in the shape of cells could be coupled to changes in their volume, we studied the evolution of cell and embryo volume with time. As our procedure involves the reconstruction of embryos fixed at

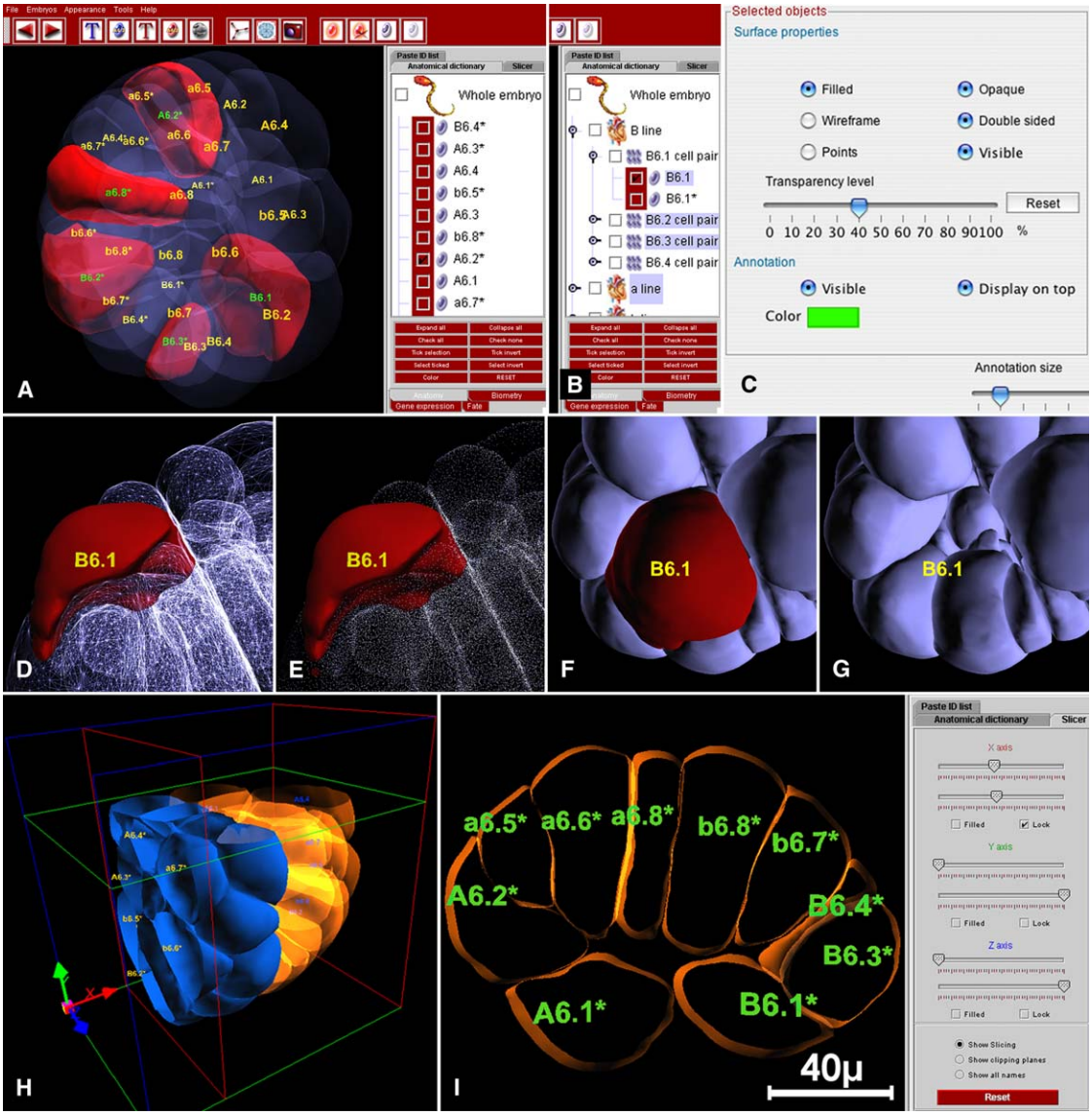

Figure 2. Visual Exploration of Embryo Structures

(A) General view of the 3D Virtual Embryo interface. The left panel shows the interactive 3D model corresponding to the same embryo as Figure 1. The right panel includes the various textual interfaces. The anatomy interface shown here simply lists structures present in the embryo model as seen in stand-alone mode.

(B) Anatomy interface organized as a hierarchical tree when 3D Virtual Embryo is used as a NISEED module.

(C) Part of the display "Display settings" interface used to change the appearance of selected objects and of their names. A similar panel allows the user to change the appearance of unselected objects.

(D and E) Wire frame (D) or points (E) representation of the cells surrounding a selected cell, revealing its outside morphology.

(F and G) Close up on a 3D model when cell B6.1 is shown (F) or hidden (G).

(H and I) Examples of the use of the slicer to reveal a model's inner structure.

different stages, it is less precise than tracking the evolution of the parameters in live embryos. For instance, the total volume of individual embryos reconstructed between the 8-cell stage, when the animal and vegetal hemispheres are first separated, and the 44-cell stage varies by up to 30% between models from different batches and by up to 20% within a batch (Figure S2E and not shown). In spite of this variability and of the drastic cell-shape changes observed between cells during these stages, the fraction of the embryo occupied by the animal or vegetal hemispheres remained very similar between the 8- and the mid 44-cell stage (Figures S4B and S2F). Thus, during cleavage stages, the volume of individual cells does not seem to be under obvious developmental control.

Another application of volume measurements is to search for unequal cleavages during embryonic cell divisions. For this, we looked for sister cells with different volumes, between the 16- and 44-cell stage of *Ciona* embryos. No asymmetric divisions were detected in the b-line cells during this period. Some potential asymmetric divisions of small amplitude, usually less than 20% of difference in the volumes of sister cells, were detected in the a- and A-lineages (Figure 5B and not shown).

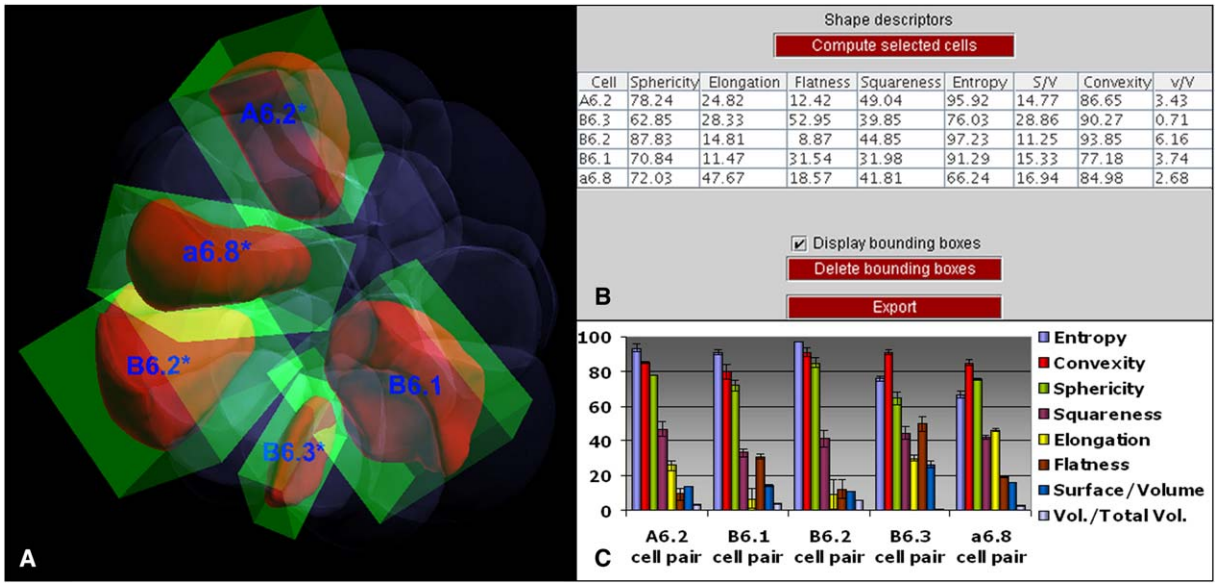

Figure 3. Cell Geometry Descriptors

(A) Visualization of bounding boxes corresponding to selected cells reflecting their relative orientation in space and their shape properties in a mid 32-cell stage embryo.

(B) View of the geometry descriptors computation interface showing the quantification of the different geometry descriptors.

(C) Graphical representation of computed descriptor values reflecting that each cell pair of an example mid-32-cell stage embryo has a characteristic geometry profile. Values for right and left symmetrical cells were averaged. Error bars represent the standard deviation.

Although these differences were always found on the left and right sides of individual embryos, they were not consistently found in all embryo models. Reconstruction of additional models, if possible from living embryos, will be required to determine whether these differences are artifactual or represent transient differences in cell volumes. The situation was clearer in the B-line cells. During cleavage stages, previous experimental work revealed the presence of asymmetric divisions in the most posterior B-line cells, a phenomenon attributed to the presence of a "centrosome attracting body" (CAB) in the posterior vegetal cortical region of the B4.1, B5.2, and B6.3 cell pairs [12]. In agreement with this work, the volumes of B5.1/B5.2 and B6.3/B6.4 sister pairs were markedly different at the 16- and 32-cell stages, respectively (not shown and Figures 5A and 5B). In addition, although their mother cells did not inherit the CAB, the volumes of the anterior-most B6.1/B6.2 sister cells showed significant differences, from their birth at the 24-cell stage to the late 32-cell stage,

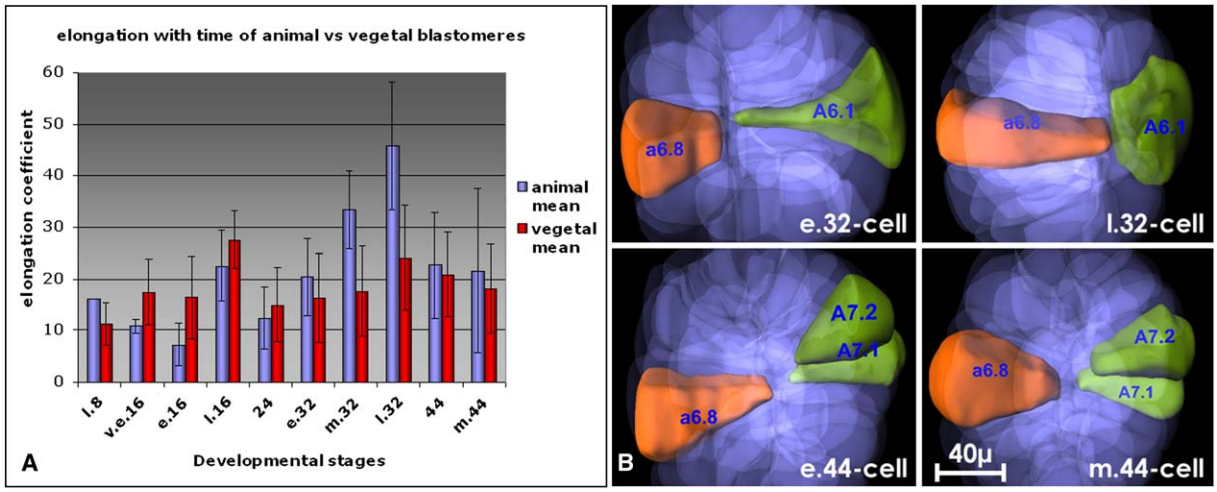

Figure 4. Evolution with Time of the Volumes and Elongation Factors of Animal and Vegetal Blastomeres

(A) Elongation with time of animal and vegetal blastomeres in single late 8-, very early 16-, early 16-, late 16-, 24-, early 32-, mid 32-, late 32-, 44-, and mid 44-cell stage embryos. The elongation coefficient was averaged for both animal and vegetal blastomeres. Error bars correspond to the standard deviation.

(B) Selection of an animal (a6.8) and an opposing vegetal (A6.1) blastomere in an early 32-cell stage embryo and their progeny in a late 32-, early 44-, and mid 44-cell stage.

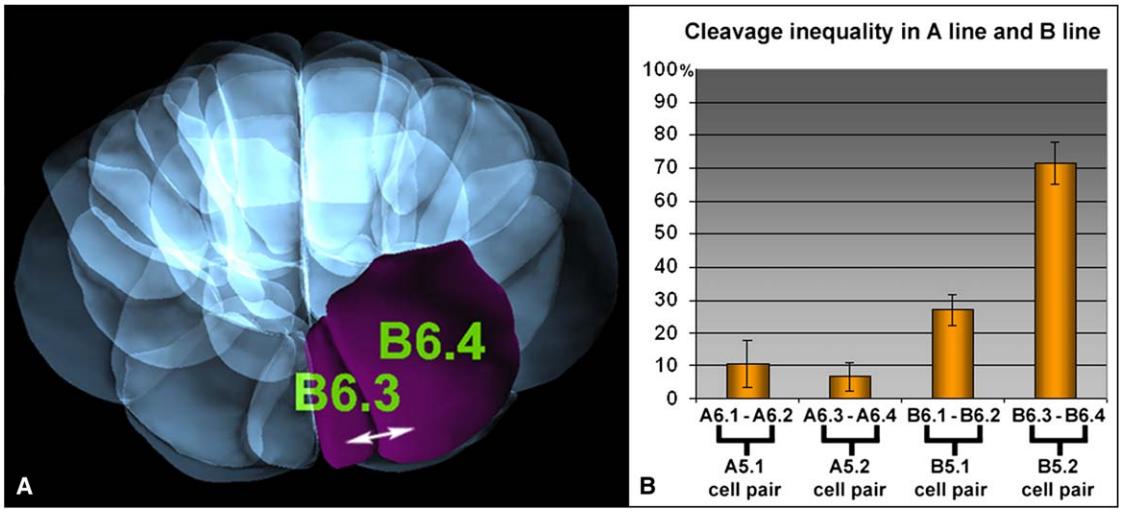

Figure 5. Cleavage Inequality in A Line and B Line Cells

(A) Visualization in 3D Virtual Embryo of two sister cells (B6.3 and B6.4) at the mid 32-cell stage presenting very different size.

(B) Quantification of the cleavage inequality in one 24-cell and six 32-cell stage embryos as measured by the formula (expressed as percentage) $I = 1 - V_A/V_B$ where cell A is smaller than cell B. For each blastomere, the volume was first averaged for each cell pair and then between the early, mid, and late 32-cell stage. The 71% value obtained for the B6.3/6.4 cell pair corresponds to a 3.7-fold difference in the volume of the two sisters. The standard deviation is represented by error bars. The figure shows that all B-line cells divide asymmetrically during their 5th somatic division.

just prior to their division (Figure 5B). The percentage of inequality of these cleavages was very robust and remarkably similar in all early 32-cell embryos, independent of their level of bilateral symmetry (Figure S2G). Furthermore, this feature was evolutionarily conserved in *Halocynthia roretzi* (not shown). At the next (44-cell) stage, B6.2 divided in turn to form an unequally sized B7.3/B7.4 sister pair (not shown). Remarkably, these novel unequal divisions all gave rise to differently fated sisters: B6.1 gives rise to endoderm, B6.2 to mesoderm, B7.3 to notochord and mesenchyme, and B7.4 to muscle. The consistency of the event in all embryos, its correlation with the acquisition of distinct fates, and its evolutionary conservation suggest that these unequal divisions may be functionally significant.

Spatial Arrangement of Blastomeres, Cellular Interfaces, and the Regulation of Inductive Processes

In parallel to the regulation of individual cell shapes, changes in the relative position of cells are a major determinant of embryo shape during and beyond gastrulation. Three distances between structures are computed by 3D Virtual Embryo and displayed in the "Distance" tab of the Biometry section: the distance between the centers of gravity of two objects (indicative of the global relative positions of structures), the minimal distance which exists between the two closest points of their surfaces (indicative of potential contacts), and the distance between the furthest points (which relates to the dimensions of the structure).

Communication between neighboring cells or structures plays a crucial role during embryonic development. The distance computation described above was therefore used to identify neighboring, and thus potentially communicating, blastomeres, those whose minimal distance falls below a given threshold (default is 5 μm) that can be adapted to the anticipated range of the signaling event (Figure 6A). In embryos with a very small cell number such as early ascidian or nematode embryos, inductive interactions are thought to occur at very short range by direct cell contact. Neighborhood relationships were thus complemented by a measure of the area of contact between neighbors (Figures 6A and 6B). By using this tool, we looked for hints that a precise regulation of the area of contact between adjacent blastomeres is important during early *Ciona* embryogenesis.

At the 32-cell stage, the *Ciona intestinalis* anterior neural tissue is induced from a-line blastomeres in response to A-line-derived FGF9/16/20 [13]. Interestingly, while all animal blastomeres (a- and b-line) are competent to respond to the inducer and while most of them contact the inducing cells, the FGF signaling pathway is activated in only 4 of 16 animal blastomeres (the a6.5 and b6.5 cell pair) in vivo [14, 15]. To look for an explanation for this restriction, we calculated the area of contact of each animal blastomere with the inducing A-line cells. To compensate for differences in size of embryos within a species, or between species, this value was normalized by dividing the measure of the area of contact between an animal blastomere and the A-line by the total surface of the animal blastomere. As presented in Figure 6C and Figure S2H, for each measured animal blastomere, this ratio was conserved between early 32- and 44-cell stages *Ciona* embryos. It was even evolutionarily conserved in a late 32-cell stage *Halocynthia* embryo, in spite of the size difference between the embryos of the two species. In all cases, a6.5 and b6.5 had the largest relative area of contact with inducing cells. This suggests that the area of contact between competent and inducing blastomeres is an important parameter to determine which cells are induced.

To further test this hypothesis, we experimentally manipulated the surface of contact between the animal

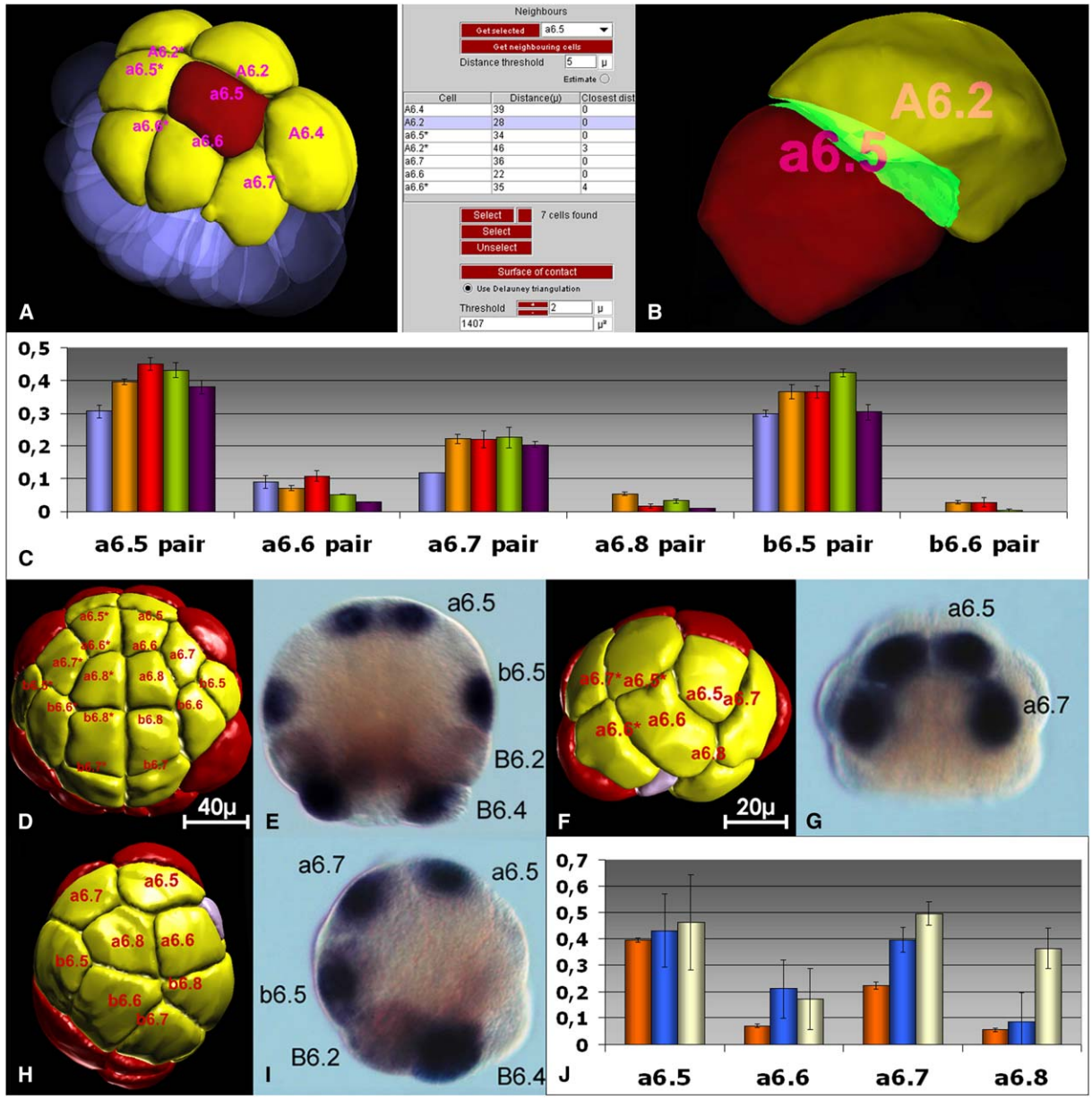

Figure 6. Differences in the Surface of Contact between Animal and A-Line Vegetal Cells

(A) General view of a6.5 and its neighbors. The right panel shows the interface used to find neighboring cells and to compute areas of contact.

(B) Visualization of the surface of contact (in green) between a6.5 and A6.2 blastomeres displayed in translucent mode.

(C) Surface of contact between individual animal cells competent to adopt a neural fate around the time of induction and the A-line blastomeres. Surfaces were normalized by dividing each value by the total surface of the animal blastomere. Areas were averaged for each cell pair. For each stage, the analysis of a single embryo is presented (blue, *Ciona* early 32-cell; orange, *Ciona* mid 32-cell; red, *Ciona* late 32-cell; green, *Ciona* early 44-cell; violet, *Halocynthia* late 32-cell). Analysis of an additional three early 32-cell and two 44-cell embryos gave similar results (Figure S2 and not shown).

(D–I) Animal views of whole embryo (D, E), anterior (F, G), and lateral (H, I) embryo halves. For each type of explant, a reconstruction at the late 32-cell stage and the expression pattern of *Ci-Otx* at the 44-cell stage are presented. Anterior is up. Animal and vegetal cells are, respectively, shown in yellow and red. The small light blue structures in the half-embryo reconstructions are tiny fragments of the removed embryo half, left during the cutting procedure.

(J) Quantification of the surface of contact between individual a-line cells and the A-line inducers. The data correspond to two reconstructed anterior halves and four lateral halves. Orange, whole embryo; blue, lateral halves; white, anterior halves. Throughout the figure, the error bars represent the standard deviation.

blastomeres and the A-line cells and monitored the effect on the anterior neural marker *Ci-Otx*. For this, we isolated at the 8-cell stage anterior (a-lines plus A-lines) or lateral (right or left) embryo halves, which were cultured either to the late 32-cell stage for reconstructions or to the 44-cell stage for the analysis of *Ci-Otx* expression (Figures 6D–6I). These half embryos developed remarkably normally, allowing the identification of

individual a- and A-line cells in the two anterior and four lateral halves that we reconstructed. The surface of contact between a-line and A-line was increased in both types of explants with a larger increase in anterior explants (Figure 6J). While the a6.7 cell established as large a contact with the A-line as the a6.5 cells in anterior and lateral explants, the surface of contact between a6.8 and the A-line was only significantly increased in anterior explants. In sibling whole embryos analyzed at the 44-cell stage (n = 317), expression of *Ci-Otx* was restricted to a6.5 and b6.5 cell pairs in 94% of embryos (Figure 6E), with 6% of embryos additionally expressing *Ci-Otx* in a6.7 cells. In sibling anterior explants, *Ci-Otx* expression was restricted to two cells (a6.5, not shown) in only 5% of explants (n = 132). In 83% of cases, marker expression was detected in 3 or 4 cells (in positions consistent with a6.5 and a6.7 identities, Figure 6G) and found in 5 cells (a6.5, a6.7, a6.8, not shown) in 10% of explants. This ectopic expression was unlikely to be due to the removal of a repressive influence emitted by the posterior lineages, as a similar increase was observed in the lateral halves (n = 209). While 38% of explants showed expression in two cells only (a6.5 and b6.5), 58% of explants expressed *Ci-Otx* in an additional cell located in between the normal two expressing cells and thus likely to be a6.7 (Figure 6I).

Thus, in both whole and bisected embryos, the surface of contact between an animal blastomere and the A-line very strongly correlated, qualitatively and quantitatively, with the expression of *Ci-Otx*, further strengthening the proposition that the area of contact between animal and inducing cells is an important parameter in the selection of induced cells. This also suggests that Ci-FGF9/16/20 acts only at very short range. Interestingly, the response to the inducer does not seem to be proportional to the surface of contact, but rather to be defined by a threshold value: while the area of contact between a6.7 and the A-line was half of that between a6.5 and the A-line in whole embryos, activation of the downstream MAP kinase ERK or of the direct transcriptional target gene *Ci-Otx* is only very rarely detected in this blastomere in *Ciona* ([14, 15] and above).

Linking Virtual Embryos to Anatomical and Genomics Data

The previous sections highlighted how 3D Virtual Embryo, used in stand-alone mode, helps identify novel developmental events. The identification of the molecular regulators of these processes requires that quantitative morphological data be put in relation with a model organism database. We therefore interfaced 3D Virtual Embryo to the Ascidian NISEED database hosting molecular, embryological, and anatomical data (O.T. et al., unpublished data).

For this, each object of a 3D embryo model was linked to the corresponding term in the NISEED hierarchical anatomical dictionary. As a consequence, the simple list of objects that appears in the "anatomy" interface in stand-alone mode is replaced by the complete hierarchical anatomical tree corresponding to the developmental stage of the model (Figure 2B). Terms close to the root of the tree represent a global structure (e.g., Mesoderm, A-line), while child terms correspond to more precise, nonoverlapping, structures (e.g., muscle, notochord, A6.2 cell pair). The user can thus simultaneously select and visualize all cells corresponding to a given cell lineage, germ layer, tissue, or organ at a given stage.

This concept was extended to the other anatomical knowledge fields of NISEED, which can be explored from 3D Virtual Embryo with the Anatomy and Fate interfaces. For example, with the "From fates to structures" interface, the user can select and visualize all cells in a model that will adopt a given destiny (Figure 7A). Conversely, the fates adopted by any selected cell or combination of cells can be obtained via the "From structures to fates" interface (Figures 7B and 7C). Likewise, one can explore lineage information in 3D. Figure 8 illustrates that the progeny of a structure selected at a given stage can be traced in models of successive developmental stages. Conversely, when switching to younger stages, the system displays the ancestors of a given structure. Should two cells displayed with different colors in the initial model share the same progenitor at an earlier stage, this progenitor blinks alternatively with the colors of the original selections (not shown).

3D Virtual Embryo can also be used as an interface to query and represent the spatial expression data from in situ hybridization experiments or *cis*-regulatory sequences included in NISEED. The simplest option, named "From gene to structures," allows the display in 3D of the expression of one or several genes, cDNA clones, or reporter constructs (Figure 9A). A different color can be allocated to each experiment displayed, and territories of overlap between expression domains alternatively blink in the corresponding colors. A second option, named "From structures to genes," identifies genes or reporter constructs expressed in a set of selected 3D structures and excluded from another (Figures 9C and 9D). The expression patterns of the identified genes can then be displayed in 3D on top of the initial selection and compared to the position of the cells of interest to the user (not shown).

3D Virtual Embryo thus constitutes a powerful interface to intuitively and didactically mine and display anatomical and molecular information included in NISEED. This is, however, just a first application of the integration of 3D and molecular data. As the number of expression profiles included in NISEED increases, it will become possible to search for and find genes specifically expressed in cells of given shapes or adopting a specific cellular behavior and thus shed light on the molecular control of these processes.

Discussion

In this article, we described a generic software aiming at quantifying the morphology, arrangement, and interactions between anatomical structures in metazoan embryos and to relate these parameters to their genetic control. By using 3D Virtual Embryo to analyze the simple *Ciona intestinalis* early cleavage embryos, we found a surprising diversity and dynamic evolution of cell shapes, we identified novel asymmetric divisions, and we provided a plausible explanation for the restriction of the induction of anterior neural tissue to a minority of animal cells. To further explore the relationships between these processes and their molecular control, we

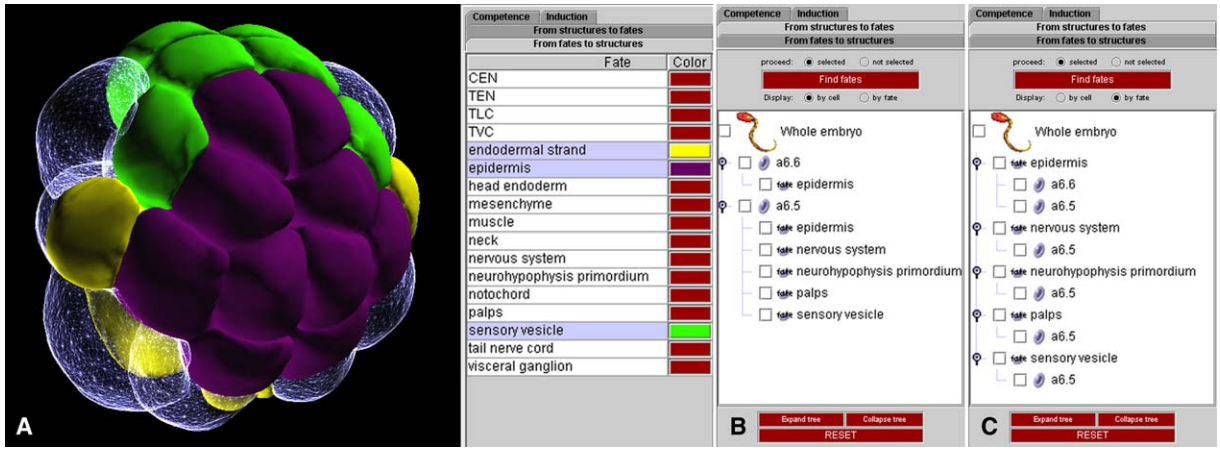

Figure 7. Exploration and Visualization of Cell Fates

(A) View of the interface "From fates to structures." The 3D panel displays the cells that will adopt the fates selected in the textual interface.
(B and C) Two different representations ([B], by cell; [C], by fate) of the results of a query for the fate of a6.6 and a6.5 using the "From structures to fates" interface.

have interfaced 3D Virtual Embryo to the NISEED database environment and presented a few examples of the advantages of this integration.

Ascidian Embryogenesis Is Driven by Cell-Autonomous Mechanisms and Very Short-Range Inductions

While ascidians have long been considered a prime example of mosaic development driven by the action of localized maternal determinants, more recent studies illustrated that, as in nematodes, inductive interactions play a crucial role in fate-specification processes [16]. Given the small embryo size and the very small number of cells present in these embryos, the spatial extent of inductive interactions has to be very precisely controlled, otherwise too many cells would adopt the same fate. Two mechanisms can be envisaged to spatially restrict the influence of an inductive clue, as exemplified during neural induction. First, competence to respond to the neural inducer is spatially limited to the animal cells by restricting the activity of a maternal transcription factor, GATAa, to the animal hemisphere [13]. Second, all

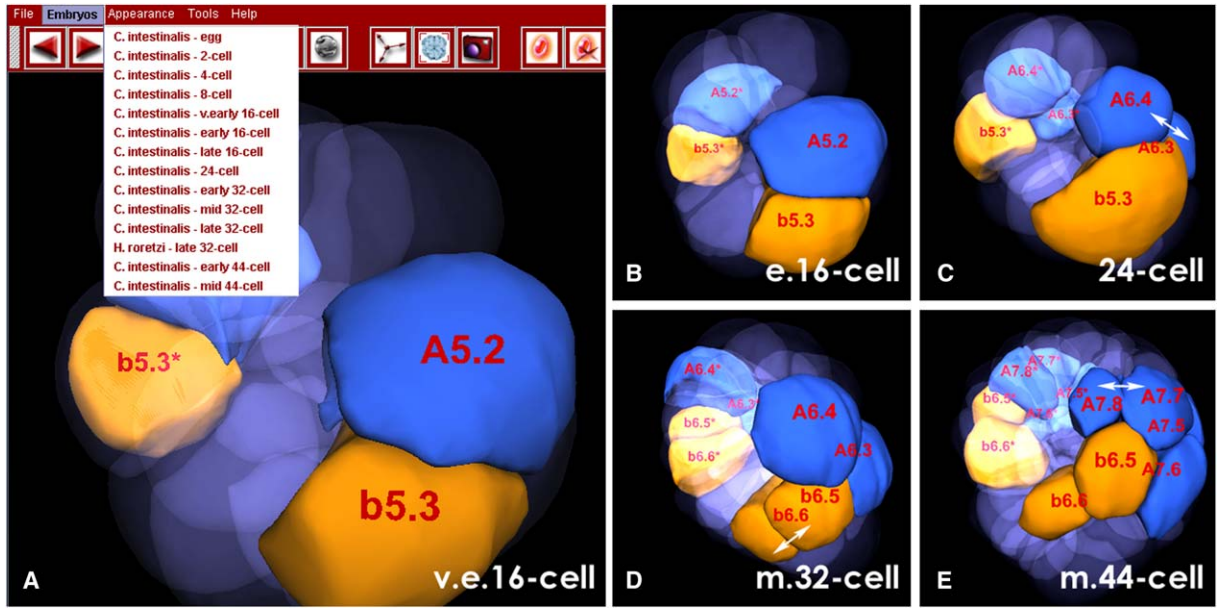

Figure 8. Exploration of Cell Lineages

(A) A very early 16-cell embryo in which cell pair b5.3 and A5.2 were selected. The panel also shows the two arrow buttons to navigate between successive stages, as well as the rolling menu with the different embryos available.
(B–E) Embryo models at the early 16-cell (B), 24-cell (C), mid 32-cell (D), and mid 44-cell (E) stages showing the position of the progeny of b5.3 and A5.2. White arrows highlight successive division events. Note that the magnification factor, orientation in space, and color settings are conserved when changing model.

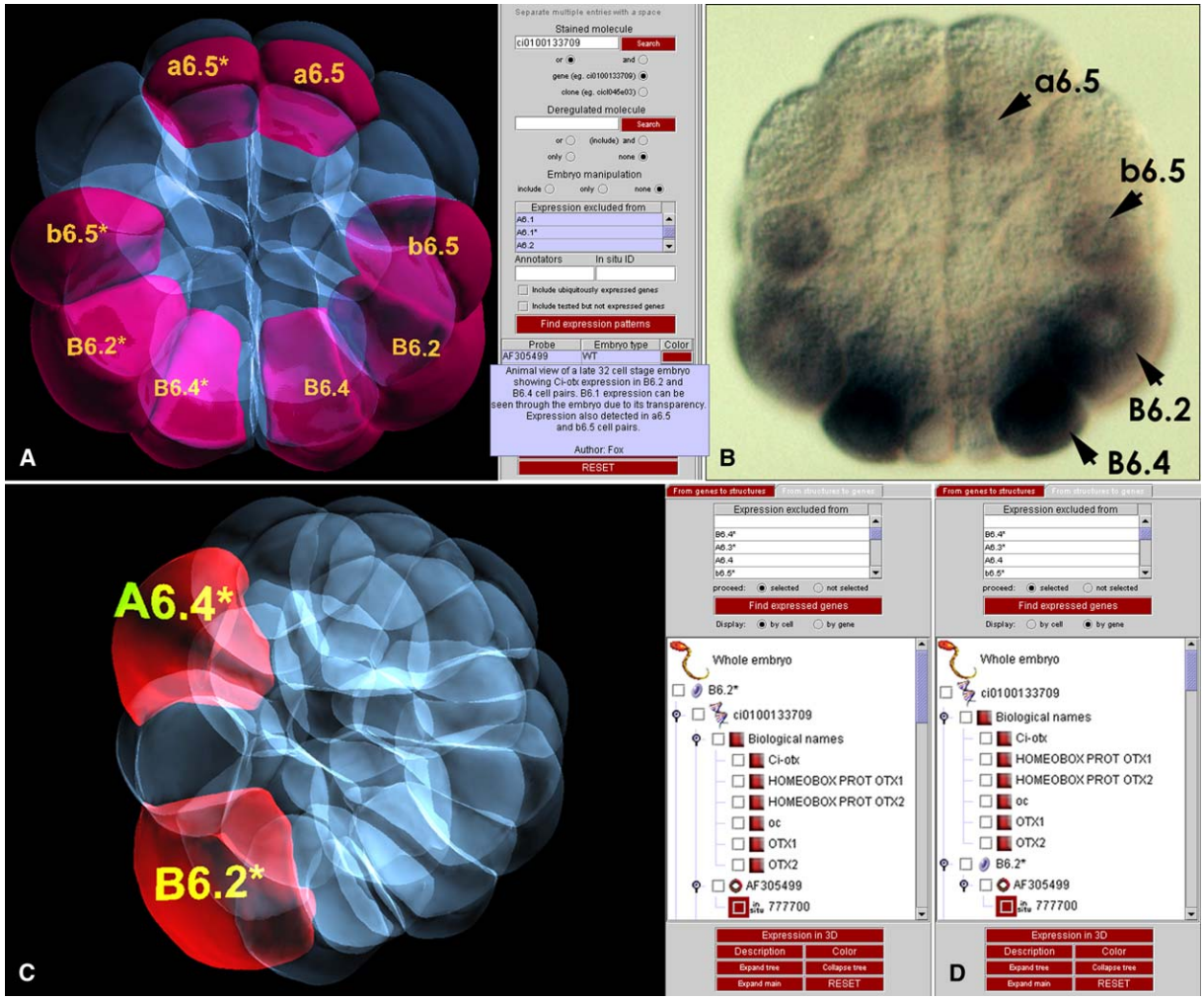

Figure 9. Exploration and Visualization of Gene Expression Data

(A) "From genes to structures" interface, showing wild-type expression of *Ci-otx* at the mid 32-cell stage. Note the menu option allowing the user to exclude genes expressed in structures deemed uninteresting, here the A-line blastomeres. A pop-up window with the NISEED textual description of the expression pattern appears upon moving the cursor over a gene's identity, guiding the user in their choice of expression patterns to be displayed in 3D.

(B) In situ hybridization picture, which was used to enter the expression pattern on *Ci-Otx* in ANISEED.

(C and D) "From structures to genes" interface showing genes expressed in selected blastomeres. The user can further restrict the query by using a rolling menu to define structures in which genes of interest should not be expressed (C). The result of the query is presented in the right hand interface panel as an expandable tree, which can be organized in two ways. By default, priority is given to the names of the selected structures, which appear at the top of the hierarchy (C). Child nodes are the genes expressed by each structure, and for each gene, its biological names and corresponding expression patterns. The alternative visualization mode (D) gives priority to the gene IDs, which appear at the top of the hierarchy. Child nodes include the associated biological names, the structures expressing the gene, and for each of these the cDNA or reporter construct used and the identifier of the corresponding NISEED data.

animal cells can respond to the inducer by activating the early neural marker *Otx* [13–15, 17]. Among these cells, only a minority adopts a neural fate, suggesting that the inducer may be spatially restricted. The data presented here suggest indeed that the extent of contact between competent and inducing cells is a key determinant of the induction. Further, our data suggest that cells do not respond linearly to the concentration of inducer, but follow a threshold response.

Toward a Quantitative Biometrical Approach to Embryonic Development

The above example, and the automatic identification of novel unequal cleavages in early *Ciona* embryos, illustrate the power of a quantitative approach to embryonic cell shapes and spatial arrangement. 3D Virtual Embryo has several unique features that distinguish it from the pioneering software in the field, 3D-DIASemb [6].

First, while 3D-DIASemb and 3D Virtual Embryo share a vectorial representation and compute morphological parameters on segmented objects, the computations they offer differ. 3D Virtual Embryo computes fewer shape descriptors than 3D-DIASemb. Yet our preliminary analysis reveals that these descriptors are sufficient to discriminate between the shapes of the different cells of early ascidian embryos. In addition to computations conceptually shared with 3D-DIASemb, 3D Virtual Embryo also computes descriptors of the interaction between cells.

Second, 3D Virtual Embryo can be used both as a stand-alone program, like 3D-DIASemb, and as a module of a model organism database, NISEED, which hosts morphological, molecular, and anatomical data. Comparison of molecular, expression, and morphological data may point to regulators of cell fate or behavior. For example, as the expression patterns of the majority of signaling ligands have been determined in *Ciona* [10], the automatic identification of the neighbors of a cell, or field of cells, expressing a given ligand, may simultaneously point to novel inductive events and to the inducer. Likewise, it should be possible to look for genes preferentially expressed in cells showing a specific geometry. This will, however, require an increase in the number of genes whose precise spatial expression pattern has been described, and which currently only represent a small minority of predicted *Ciona* gene models.

Genericity of 3D Virtual Embryo and Use with Different Model Organisms

Use of 3D Virtual Embryo and NISEED is not restricted to ascidian embryos. Both systems were designed as generic software adaptable to a variety of model organisms. The biological system used in this article, the *Ciona* embryo, has the peculiarity of being small and developing with very few cells and with a fixed lineage. It thus offers cellular resolution. Other systems share these characteristics and would be ideally suited for a morphological analysis of their development with 3D Virtual Embryo. These include, for instance, the nematode *Caenorhabditis elegans* because of its very small embryo size and the existence of transgenic lines expressing membrane-tagged GFPs [18] and of a rich body of embryological and molecular data that can be confronted to morphological analysis. As in *Ciona*, inductions in *C. elegans* are thought to occur at short range, and it would be interesting to test whether the area of contact between blastomeres is also an important parameter. The Appendicularian *Oikopleura dioica*, another invertebrate chordate, is also thought to develop with an invariant lineage (reviewed in [19]). This lineage has, however, not been described in detail, in part because the cleavages are very rapid and deviate from bilaterality. As a result, cell identities are very difficult to recognize. Use of 3D Virtual Embryo, which provides for each cell a morphological footprint, should ease the description of the appendicularian lineages by allowing recognition of identical cells in different embryos.

Embryos developing with a large cell number can also benefit from 3D Virtual Embryo. The level of resolution used can be adapted to the characteristics of the embryo and to the precision of the anatomical ontologies defined for each model organism. In complex embryos developing with large number of cells, the structures reconstructed will probably be at the level of the tissue types (notochord, muscle, neural plate). Likewise, the threshold for the detection of "neighbors" can be adjusted to take into account that in some embryos, inductive signals can travel over several cell diameters. As the procedures used to reconstruct embryo models vary with the size and complexity of the embryos considered, we chose not to include in the package any software to reconstruct embryos in 3D.

Future Prospects

This work presented the application of 3D Virtual Embryo to describe normal pregastrula *Ciona* development. The next logical step will be to generate the first detailed description of the evolution of cell shapes and trajectories during gastrulation. Another very interesting application of this software will be to quantify the effect of genetic or embryological perturbations on embryo morphology and morphogenesis. While this could already be done with very early embryos injected with Morpholino antisense oligonucleotides or electroporated with various constructs, a limiting factor for this type of studies is the tediousness of manual reconstruction of embryo models, reconstruction of a 44-cell embryo taking about a full day. Automatic or semiautomatic segmentation algorithms have been described [20, 21] and can be successfully used in ascidians to segment nuclei or other isolated subcellular structures (not shown). The quality of the phalloidin staining we used is, however, not sufficient to automatically reconstruct individual cells boundaries. We are currently developing membrane-targeted GFPs, which should improve the quality of the image stacks by increasing the contrast between membrane and cytoplasm. Such markers would additionally allow users to image live embryos.

Finally, a quantitative description of cell shapes and behaviors opens the way to the mathematical modeling of the mechanical constraints that determine the shape and position of each cell and hence the morphology of the embryo.

Experimental Procedures

System Requirements

3D Virtual Embryo can be downloaded under GNU Lesser General Public License at http://aniseed-ibdm.univ-mrs.fr/~ciona/ANISEED/virtual_embryo.php. It is written in Java and requires java 1.4 and java3D 1.3.1 or above (see the web site for the installation procedure). 3D Virtual Embryo is multiplatform and has been successfully tested under MacOs 10.3, Windows 2000/XP, and Linux Mandrake 10.

Generation and Staging of Embryos

Animals were collected in the Brest harbour by divers from the Marine Biology Station in Roscoff (France) and kept under constant light in Marseille. Embryos were obtained by in vitro fertilization and reared at 17ºC to 18ºC. Staging was done according to the number of cells in embryos, two consecutive stages being separated by at most 20 min. Substages of the 16- and 32-cell stages were defined according to the external shape of the embryo. Substages of the 44-cell embryos were defined by observing the phase of the cell cycle of animal cells, as determined by the observation of DAPI-stained chromatids: animal cells of early 44-cell embryos are in prophase, those of mid 44-cell are in metaphase, and those of late 44-cell are in anaphase. Embryos were fixed for 3–10 min at 17ºC–18ºC in HEPES-buffered Artificial Seawater (ASWH) containing 4% formaldehyde and immediately stained with tritc-phalloidin (Sigma, P-1951).

Embryo Reconstruction and Segmentation

Confocal z-stacks, in which distances between optical sections were set at 1 μm, of fixed embryos stained with tritc-phalloidin and mounted in PBS, were obtained with a 40x Plan-Neofluar oil immersion objective on a biphoton LSM510 META ZEISS confocal microscope equipped with an Amplitude laser with a 1030 nm wavelength. Because of the optical aberration created by the difference in refraction indices between the immersion oil and the PBS in which the samples were mounted, embryos appeared thicker than in reality. This was corrected according to [22] by shortening the z-axis by

a factor of 0.8528. After this correction, imaged eggs were spherical (not shown). Likewise, early 32-cell embryos, which, alive, appear spherical under the dissecting scope, also had a spherical shape after the reconstruction. The use of an oil-immersion objective on samples mounted in an aqueous medium also led to the blurring of the parts of the embryo that were most distant from the objective (not shown). We could not correct this spherical aberration, but the blurring was not sufficiently severe as to compromise the identification of cell boundaries. This aberration will be avoided in the future by the use of a water immersion objective. From these image stacks, the outer surface of each blastomere was reconstructed as a polygonal mesh via the MeasurementPro module of Imaris (Bitplane, AG) or the 3D segmentation editor of Amira. Both softwares gave similar results (not shown). Reconstructed 3D objects were exported as an Open Inventor (IV) file (bitplane) or VRML file (Amira) and converted in the 3ds format with "Ivcon" and "3D exploration" (Xdimension software, LLC) software. This file was edited with Gmax 1.2 (Autodesk) to name cells, correct surface artifacts, and orient the embryo. The editor software was next used to generate two versions of each model, differing in the size and density of polygons in the mesh, without visibly altering the shape of the object. The high-resolution model is used to make quantitative measurements on the geometry of individual structures. The low-resolution model allows the software to run on modest computers and is sufficient to be used for a visual examination of embryos, to query the database, or to display results from such queries. A smooth display of 3D objects was obtained for both versions by averaging the normal vectors of neighboring polygons (Figure 1D). The resulting 3D embryo models were exported as a MD3 file, by using the Gmax MD3 export plug-in. The final OBJ format file was obtained with "3D exploration."

Upon loading of a 3D object, 3D Virtual Embryo verifies whether the mesh is made of polygons or triangles, and if necessary, decomposes each polygon into triangles to simplify the calculation of biometry measurements. At this step, each triangle ABC is oriented by defining a normal N_{ABC} using the order of the vertices and the right-hand rule, so that triangles on opposite sides of the object will have opposite orientations (Figure 1D).

Measure of the External Surface of an Object

The measure of the area of an object is estimated in μm^2 by an algorithm, which calculates the sum of the surfaces of the triangles composing the object's surface with the Heron formula, according to which the surface S of a triangle ABC is:

$$S = \sqrt{p(p-a)(p-b)(p-c)},$$

in which a, b, and c represent the distances CB, CA, and AB, respectively, and p is the half perimeter of the triangle.

Calculation of the Volume of an Object

The algorithm used calculates the volume of the object by summing the signed volumes of a set of pyramids [23]. Starting from an origin O, the software constructs for each triangle ABC of the mesh, with A(x1, y1, z1), B(x2, y2, z2), and C(x3, y3, z3), the tetrahedron having this triangle as a base and O as summit. The signed measure of the volume of each pyramid (V_{pyr}) is calculated by the formula

$$V_{pyr} = \frac{1}{6}(-x_3y_2z_1 + x_2y_3z_1 + x_3y_1z_2 - x_1y_3z_2 - x_2y_1z_3 + x_1y_2z_3).$$

By this calculation, individual volumes have a negative sign when the normal of the triangle points toward O and a positive sign otherwise. The total volume of the object is the sum of the signed volumes of all tetrahedrons.

Calculation of the Inequality of Cleavage between Sister Cells

The inequality of cleavage (Uc) is computed by comparing the volume of two sister cells A and B. If A has larger volume than B, we calculate

$$Uc = 1 - \frac{V_B}{V_A},$$

which is expressed as a percentage.

Calculation of the Area of Contact between 3D Objects

3D Virtual Embryo first computes the distance between each couple of points on the two neighboring objects and selects the points of each mesh that are closer than a user-specified threshold (default is 4 μm) from the other object. Once a point is selected, the triangles it belongs to in the mesh are kept in memory and used to display, on each object, the surface of contact in 3D. As an alternative calculation, 3D Virtual Embryo uses the selected points to link them and create new triangles to reconstruct the surface of contact by a standard Delaunay triangulation algorithm [24]. This second approach is less sensitive to the resolution of the model, but it is unsuitable to compute irregular contacts. Once the surface of contact is reconstructed, its area is calculated by the Heron formula as above.

Principal Components Analysis

The first step of this procedure is to determine for each object a local referential, centered on the object's center of gravity, and defined by the object's principal axes, which correspond to the three orthogonal main axes of the smallest ellipsoid enclosing the object. If all triangles of mesh were of equal size, the center of gravity of each object would be calculated as the point having coordinates equal to the mean of the coordinates of all centers of gravity of the triangles. Triangles, however, have different sizes. To correct this effect, the center of gravity of the mesh was calculated by weighing the center of gravity of each triangle by the surface of the triangle. With this point as an origin, the matrix M of the coordinates of the n vertices on the 3D mesh surface of the object is created and its 3 × 3 covariance matrix M′ computed. The principal axes are defined by the three orthonormal eigenvectors $\vec{\zeta}i = (xi, yi, zi)$, i = 1, 2, 3 of the covariance matrix M′:

$$M' \times \vec{\zeta}i = \lambda i \vec{\zeta}i,$$

and

$$xi^2 + yi^2 + zi^2 = 1, \text{for } i = 1, 2, 3$$

where λ_i are the eigenvalues. These equations define three orthonormal eigenvectors, one along each principal axis of the enclosing ellipsoid and three eigenvalues.

Defining the Best-Fitting Bounding Box and Convex Hull of an Object

Eigenvectors are used to compute a bounding box defined as the smallest square box including an object (Figure 3A). Its edges are parallel to the three principal axes of the object. Its boundaries are defined by the largest coordinates of object vertices along each of the six half-lines defined by the principal axes. To define the convex hull of each object, Qhull was integrated into 3D Virtual Embryo, and the coordinates of the convex hull of each object were calculated as described in [25].

Computation of Geometry Descriptors

3D Virtual Embryo computes eight 3D geometry descriptors characterizing the "Entropy," "Squareness," "Elongation," "Flatness," "Sphericity," "Convexity," "Surface over volume" (or "S/V") ratio, and "Fractional Occupancy" of an object.

The entropy of an object provides a measure of its compactness. It was calculated from the object's eigenvalues λ_i (i = 1, 2, 3) along the principal axes. If we define:

$$pi = \frac{\lambda i}{\lambda 1 + \lambda 2 + \lambda 3}; i = 1, 2, 3,$$

the entropy m_{entrop} is calculated by:

$$m_{entrop} = \frac{1}{\log 3} \times \sum_{i=1}^{3} pi \log(pi).$$

m_{entrop}, expressed as a percentage, is comprised between 0 and 100 for any shape. It is null for a straight line and equals 100 for a perfect sphere.

The squareness factor, Sq, is computed by comparing the volume of the bounding box to the corresponding object:

$$S_q = \frac{V_{object}}{V_{box}} \times 100.$$

Measures of the elongation and flatness of an object are computed by comparing the lengths e_{max}, e_{mid}, and e_{min} of the three

edges of its bounding box. A box is defined as elongated if the length e_{max} of the longest edge is significantly larger than e_{mid} of the intermediate edge. Conversely, an object is considered flat if the length e_{min} of the shortest edge is significantly shorter than e_{mid} of the intermediate edge. We therefore defined

$$m_{elong} = 1 - \frac{e_{max}}{e_{mid}}$$

and

$$m_{flat} = 1 - \frac{e_{mid}}{e_{min}},$$

which are expressed as percentages.

To calculate the sphericity of an object, we chose among several methods that of Silva and colleagues [26], which gave best agreement with the apparent sphericity of the embryonic blastomeres:

$$Sph = \frac{6\sqrt{\pi}V}{S^{3/2}},$$

where S is the surface of the object and V its volume.

The convexity of an object was computed as the ratio of the volume of the object over the volume of its convex hull. A value of 1 means the object is convex, and this value decreases with the apparition of concave domains.

The S/V ratio was calculated by dividing the surface of the object by its volume, while the fractional occupancy, which provides a measure of portion of the embryo a cell occupies, is calculated by dividing the volume of the cell by the sum of the volumes of all cells, taken as a measure of the total embryo volume, as early ascidian embryos have no coelomic cavities.

Supplemental Data

Supplemental Data include four figures, one movie, and Supplemental Experimental Procedures and can be found with this article online at http://www.current-biology.com/cgi/content/full/16/4/345/DC1/.

Acknowledgments

We thank Zeiss for lending us the 2-photon LSM510 confocal microscope used to image *Ciona* embryos, and J.M. Lago (C. Zeiss) and P. Weber (IBDM) for their kind availability and expert assistance with this microscope. The late 32-cell stage *Halocynthia* embryo was reconstructed from an image stack acquired in the laboratory of H. Saiga (Tokyo Metropolitan University, Japan) during a visit from V.B. We are grateful to A. Sidow (Stanford University, CA), M. Zernicka-Goetz (Cambridge University, UK), and members of our Institute and research team for critical reading of the manuscript and to all members of our team for constructive discussions during the course of this work. Special thanks to F. Robin for helpful discussion on the mathematical descriptors and shape clustering and to E. Drula for her help with the reconstruction of explants. R. Lima (Centre de Physique Théorique, Marseille) greatly helped us with the principal component analysis. We thank the Model Systems Service of the Roscoff Marine Biology Station for collecting the animals we use and F. Graziani for help with their maintenance. This work was supported by CNRS, the Ministry of Research (ACI programme and GIS "Génomique Marine"), the Marseille-Nice Genopôle, the ARC, and a framework 5 European Network, "Embryos against Cancer" (QLK3-CT-2001-01890). V.B. was supported by a fellowship from the "Fondation pour la Recherche Médicale" and O.T. by "Embryos against Cancer" and by a fellowship from the Association pour la Recherche sur le Cancer.

Received: August 17, 2005
Revised: December 23, 2005
Accepted: December 27, 2005
Published: February 21, 2006

References

1. Davidson, E.H., Rast, J.P., Oliveri, P., Ransick, A., Calestani, C., Yuh, C.H., Minokawa, T., Amore, G., Hinman, V., Arenas-Mena, C., et al. (2002). A genomic regulatory network for development. Science *295*, 1669–1678.
2. Levine, M., and Davidson, E.H. (2005). Gene regulatory networks for development. Proc. Natl. Acad. Sci. USA *102*, 4936–4942.
3. Leptin, M. (2005). Gastrulation movements: the logic and the nuts and bolts. Dev. Cell *8*, 305–320.
4. Pilot, F., and Lecuit, T. (2005). Compartmentalized morphogenesis in epithelia: from cell to tissue shape. Dev. Dyn. *232*, 685–694.
5. Baldock, R.A., Bard, J.B., Burger, A., Burton, N., Christiansen, J., Feng, G., Hill, B., Houghton, D., Kaufman, M., Rao, J., et al. (2003). EMAP and EMAGE: a framework for understanding spatially organized data. Neuroinformatics *1*, 309–325.
6. Heid, P.J., Voss, E., and Soll, D.R. (2002). 3D-DIASemb: a computer-assisted system for reconstructing and motion analyzing in 4D every cell and nucleus in a developing embryo. Dev. Biol. *245*, 329–347.
7. Dehal, P., Satou, Y., Campbell, R.K., Chapman, J., Degnan, B., De Tomaso, A., Davidson, B., Di Gregorio, A., Gelpke, M., Goodstein, D.M., et al. (2002). The draft genome of *Ciona intestinalis*: insights into chordate and vertebrate origins. Science *298*, 2157–2167.
8. Vinson, J.P., Jaffe, D.B., O'Neill, K., Karlsson, E.K., Stange-Thomann, N., Anderson, S., Mesirov, J.P., Satoh, N., Satou, Y., Nusbaum, C., et al. (2005). Assembly of polymorphic genomes: algorithms and application to *Ciona savignyi*. Genome Res. *15*, 1127–1135.
9. Satou, Y., Takatori, N., Fujiwara, S., Nishikata, T., Saiga, H., Kusakabe, T., Shin-i, T., Kohara, Y., and Satoh, N. (2002). *Ciona intestinalis* cDNA projects: expressed sequence tag analyses and gene expression profiles during embryogenesis. Gene *287*, 83–96.
10. Imai, K.S., Hino, K., Yagi, K., Satoh, N., and Satou, Y. (2004). Gene expression profiles of transcription factors and signaling molecules in the ascidian embryo: towards a comprehensive understanding of gene networks. Development *131*, 4047–4058.
11. Conklin, E.G. (1905). The organization and cell-lineage of the ascidian egg. J. Acad. Nat. Sci. Philadelphia *13*, 1–119.
12. Hibino, T., Nishikata, T., and Nishida, H. (1998). Centrosome-attracting body: a novel structure closely related to unequal cleavages in the ascidian embryo. Dev. Growth Differ. *40*, 85–95.
13. Bertrand, V., Hudson, C., Caillol, D., Popovici, C., and Lemaire, P. (2003). Neural tissue in ascidian embryos is induced by FGF9/16/20, acting via a combination of maternal GATA and Ets transcription factors. Cell *115*, 615–627.
14. Hudson, C., and Lemaire, P. (2001). Induction of anterior neural fates in the ascidian *Ciona intestinalis*. Mech. Dev. *100*, 189–203.
15. Hudson, C., Darras, S., Caillol, D., Yasuo, H., and Lemaire, P. (2003). A conserved role for the MEK signalling pathway in neural tissue specification and posteriorisation in the invertebrate chordate, the ascidian *Ciona intestinalis*. Development *130*, 147–159.
16. Nishida, H. (2002). Patterning the marginal zone of early ascidian embryos: localized maternal mRNA and inductive interactions. Bioessays *24*, 613–624.
17. Darras, S., and Nishida, H. (2001). The BMP/CHORDIN antagonism controls sensory pigment cell specification and differentiation in the ascidian embryo. Dev. Biol. *236*, 271–288.
18. Rolls, M.M., Hall, D.H., Victor, M., Stelzer, E.H., and Rapoport, T.A. (2002). Targeting of rough endoplasmic reticulum membrane proteins and ribosomes in invertebrate neurons. Mol. Biol. Cell *13*, 1778–1791.
19. Nishino, A., and Satoh, N. (2001). The simple tail of chordates: phylogenetic significance of appendicularians. Genesis *29*, 36–45.
20. Kass, K., Witkin, A., and Terzopoulos, D. (1988). Snakes: active contour models. Int. J. Comput. Vis. *1*, 321–332.
21. Pham, D.L., Xu, C., and Prince, J.L. (2000). Current methods in medical image segmentation. Annu. Rev. Biomed. Eng. *2*, 315–337.
22. Kuypers, L.C., Decraemer, W.F., Dirckx, J.J., and Timmermans, J.P. (2005). A procedure to determine the correct thickness of an object with confocal microscopy in case of refractive index mismatch. J. Microsc. *218*, 68–78.
23. Zhang, D., and Chen, T. (2001). Efficient feature extraction for 2D/3D objects in mMesh representation. Proc. Intl. Conf. Image Processing *3*, 935–938.

24. Delaunay, B. (1934). Izvestia Akademii Nauk SSSR. Otdelenie Matematicheskikh i Estestvennykh Nauk. *7*, 793–800.
25. Barber, C.B., Dobkin, D.P., and Huhdanpaa, H.T. (1996). The Quickhull algorithm for convex hulls. ACM Trans. Math. Softw. *22*, 469–483.
26. Silva, A.C., Carvalho, P.C., and Gattass, M. (2005). Diagnosis of lung nodule using semivariogram and geometric measures in computerized tomography images. Comput. Methods Programs Biomed. *79*, 31–38.